Research Article

An efficient approach for prediction of the nonlocal critical buckling load of double-walled carbon nanotubes using the nonlocal Donnell shell theory

Abdelaziz Timesli[1,2]

Received: 21 November 2019 / Accepted: 4 February 2020 / Published online: 14 February 2020

Abstract
This paper aims to apply the nonlocal Donnell shell theory to study the buckling of double-walled carbon nanotubes (DWCNTs) under axial compression taking into account the effects of internal small length scale and the Van der Waals interactions between layers. The DWCNTs is modeled as nonlocal double circular cylindrical elastic shells. On the basis of nonlocal elasticity theory, governing equations for buckling of Donnell shells are obtained taking into account the Van der Waals force. The nonlocal buckling load of DWCNT is derived without any assumption on radius tubes. However, it is a very difficult task to obtain the analytical solution of nonlocal critical buckling load. In this paper, we develop an approach for prediction of the nonlocal critical buckling load of DWCNTs.

Keywords Buckling · Double-walled carbon nanotubes · Van der Waals interaction · Axial compression · Small scale effect · Nonlocal elasticity theory · Donnell shell theory

1 Introduction

Nanostructures are increasingly used in the micro/nano-scale and systems such as the biosensor, atomic force microscope, micro-electro-mechanical, and nano-electro-mechanical systems due to their superior electronic and mechanical properties. In such applications, the effects are experimentally observed in a small scale, these effects are important and must be considered when studying their behavior.

Thin-shell theories are applied successfully basing on continuum mechanics for single-walled and double-walled carbon nanotubes (SWCNTs, DWCNTs) to predict several mechanical properties. For SWCNTs and DWCNTs models, the elastic Donnell shell has been chosen in these references [14, 35–39, 44, 48, 53]. These conventional models of shell based on classical continuous medium theories are not able to describe the effects due to the lack of small scale parameters of the material. In classical theory of local elasticity, the stresses tensor at a structure point is a function of the strain tensor of this point. However, Eringen [10, 12] pointed out that when we examine a small scale structure, the medium can no longer be considered as continuous and the internal characteristic lengths, such as the carbon-carbon bond in the carbon nanotube, must be considered. This motivation is a powerful incentive for Eringen to develop a nonlocal elasticity theory. This theory initiated by Eringen [10], is one of the promising theories that takes into account the size of small scales. The nonlocal elasticity theory implies that the stresses tensor at a point is estimated as a function of the strain tensor in the considered point and strain tensors at all other structure

✉ Abdelaziz Timesli, ABDELAZIZ.TIMESLI@univh2c.ma; abdelaziz.timesli@gmail.com | [1]Hassan II University of Casablanca, National School of Arts and Crafts of Casablanca (ENSAM Casablanca), 150 Avenue Nile Sidi Othman, 20670 Casablanca, Morocco. [2]Applied Sciences Laboratory (Laboratoire des Sciences Appliquées LSA), National School of Applied Sciences of Al-Hoceima (ENSA d'Al-Hoceima), Abdelmalek Essaâdi University, BP 03, Ajdir, Al-Hoceima, Morocco.

points. In this way, the small scale effects are understood through the use of the governing behavior laws which are based on the nonlocal elasticity theory. The nonlocal effect in the analysis is determinate by a constant appropriate to each material as defined by Eringen [10–12], this constant is called the nonlocal parameter as well as denoted by e_0. There are several works in the literature based on the nonlocal continuum theory of Eringen. Kiani [18] studied the axial buckling of a set of SWCNTs aligned vertically in two orthogonal directions. The same researcher Kiani [20] calculated the axial buckling load of the nanosystem using Euler-Bernoulli beam theory, then by implementing Galerkin approach and assumed mode methodology. Hussain et al. [16] indicated that the nonlocal theory play an important role in predicting SWCNT frequencies. The nonlocal Eringen theory is still used by the researchers in recent years [6, 16, 20, 42, 43]. Another group of non-classical theories, which have attracted the researcher's attention, is the strain gradient and couple stress theories [24–27, 30–33].

The static, buckling and vibration behaviors of nanosystems are of great interest and special attention by the applied mechanics community as shown these recent works [9, 21–23, 45]. In this context, on the basis of the nonlocal elasticity theory, we propose use the nonlocal Donnell shell theory to study the buckling of DWCNTs subjected to an axial pressure taking into account the effects of internal small length scale and the interactions of Van der Waals between layers. Through this work, a novel approach for the nonlocal critical buckling load of DWCNT is developed.

2 Donnell shell model based on the nonlocal elasticity theory.

In the Donnell shell model [8], the induced stresses are given in the median surface of the shell and the terms of the order $\frac{1}{n^2}$ are neglected, where n is the circumferential half wavenumber. So in this paper, the assumption $\frac{1}{n^2} \ll 1$ has been used where the value of n must be greater than 4. On the other hand the thin shell assumption $\left(\frac{h}{R}\right)^2 \ll 1$ has been used in the derivation, then transverse-shear and rotary-inertia effects have been neglected. In addition, the shear deformation effect is more significant in the low aspect ratio *length*/*radius* ($= \frac{L}{R}$) of nanotubes. So the other assumption $\frac{L}{R} \geq 10$ has been used in this paper.

2.1 Equilibrium equations

Consider a thin-walled circular cylindrical shell of length L, wall thickness h and a middle surface of radius R with $h \ll R$ (see Fig. 1). The shell is made of an elastic homogeneous isotopic material of Young modulus E and Poisson ratio ν.

The middle surface of the shell is referred to cylindrical coordinates x, θ and z. The distance from the middle surface is measured by the coordinate z. We note by u_x, u_θ and u_z the displacement components in the axial (x), circumferential (θ) and radial (z) directions respectively. We assume that the shell is subjected to an external pressure $p = p(x, \theta)$. Using theory of the first shear deformation, the displacements are given by:

$$\begin{aligned} u_x(x,\theta,z) &= u(x,\theta) - z\frac{\partial w}{\partial x} \\ u_\theta(x,\theta,z) &= v(x,\theta) - \frac{z}{R}\frac{\partial w}{\partial \theta} \\ u_z(x,\theta,z) &= w(x,\theta,z) \end{aligned} \tag{1}$$

where u, v and w are the reference surface displacements.

The kinematic relations for normal strain ε_{xx} and $\varepsilon_{\theta\theta}$ and shear strain $\gamma_{x\theta}$ are expressed by:

$$\begin{aligned} \varepsilon_{xx} &= \frac{\partial u}{\partial x} + \frac{1}{2}\left(\frac{\partial w}{\partial x}\right)^2 \\ \varepsilon_{\theta\theta} &= \frac{1}{R}\frac{\partial v}{\partial \theta} + \frac{w}{R} + \frac{1}{2R^2}\left(\frac{\partial w}{\partial \theta}\right)^2 \\ \gamma_{x\theta} &= \frac{\partial v}{\partial x} + \frac{1}{R}\frac{\partial u}{\partial \theta} + \frac{1}{R}\frac{\partial w}{\partial x}\frac{\partial w}{\partial \theta} \end{aligned} \tag{2}$$

The Donnell nonlinear equilibrium equations of the thin-walled circular cylindrical shell are given by [17]:

$$\begin{aligned} &\frac{\partial N_x}{\partial x} + \frac{1}{R}\left(\frac{\partial N_{x\theta}}{\partial \theta}\right) = 0 \\ &\frac{\partial N_{x\theta}}{\partial x} + \frac{1}{R}\left(\frac{\partial N_\theta}{\partial \theta}\right) = 0 \\ &\frac{\partial^2 M_x}{\partial x^2} + \frac{2}{R}\frac{\partial^2 M_{x\theta}}{\partial x \partial \theta} + \frac{1}{R^2}\frac{\partial^2 M_\theta}{\partial \theta^2} \\ &\quad + \frac{N_\theta}{R} + N_x\frac{\partial^2 w}{\partial x^2} + \frac{2N_{x\theta}}{R}\frac{\partial^2 w}{\partial x \partial \theta} + \frac{N_\theta}{R^2}\frac{\partial^2 w}{\partial \theta^2} + p = 0 \end{aligned} \tag{3}$$

where N_x and N_θ are the normal forces, $N_{x\theta}$ is the internal shear force, M_x and M_θ are the bending moments and $M_{x\theta}$

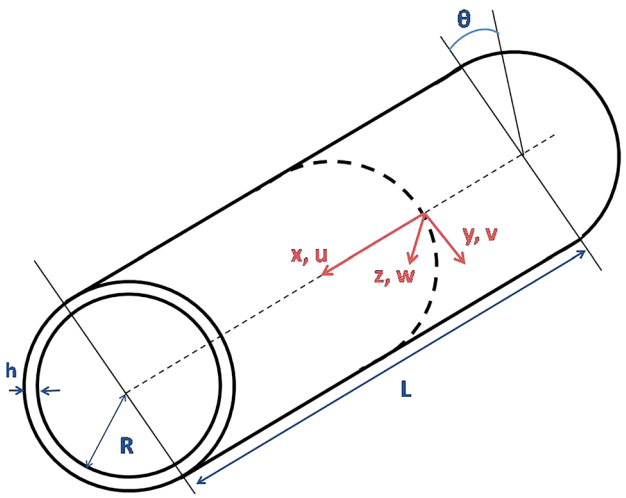

Fig. 1 Thin-walled circular cylindrical shell

is the twisting moment, which are related to internal stress σ_x, σ_θ and $\tau_{x\theta}$ by the following integrals:

$$\begin{aligned} N_x &= \int_{-h/2}^{h/2} \sigma_{xx} dz, \quad N_\theta = \int_{-h/2}^{h/2} \sigma_{\theta\theta} dz, \\ N_{x\theta} &= \int_{-h/2}^{h/2} \tau_{x\theta} dz \\ M_x &= \int_{-h/2}^{h/2} z\sigma_{xx} dz, \quad M_\theta = \int_{-h/2}^{h/2} z\sigma_{\theta\theta} dz, \\ M_{x\theta} &= \int_{-h/2}^{h/2} z\tau_{x\theta} dz \end{aligned} \tag{4}$$

2.2 Nonlocal elasticity theory and Donnell shell theory

To take small scale effects into consideration in the buckling analysis of the Donnell cylindrical shell, we apply the nonlocal elasticity theory introduced by Eringen [10, 12]. This is a semi-empirical theory based on the atomic theory and experimental observations. It assumes that the stress tensor at each point of the continuum body depends on the strain tensor at that point and also the strains at all neighboring points of the body. However, in the macroscopic (local) elasticity theory, the stress at each point depends only on the strain at that point. To express the nonlocal stress at each point x for homogeneous isotropic material, Eringen proposed the following constitutive equation :

$$\sigma_{ij}^{nl} = \int_V \alpha(|x' - x|, \tau) C_{ijkl} \varepsilon_{kl}(x') dV(x') \tag{5}$$

where σ_{ij}^{nl} is the nonlocal stress tensor, $|x' - x|$ is the Euclidian distance, C_{ijkl} is the elastic modulus, ε_{kl} is the strain tensor, $\alpha(|x' - x|, \tau)$ is the kernel function having the length dimension and expresses the nonlocal modulus into the constitutive equation, $\tau = \frac{e_0 a}{\ell}$ with a is an internal characteristic length (carbon-carbon bonds lengths, granular distance... etc.), ℓ is an external characteristic length (rupture length, wavelength... etc.) and e_0 is an appropriate constant depends on the considered material. Consequently, another characteristic length e_0 influences on predictions in nonlocal elasticity theory. It is often difficult to find an explicit expression of the kernel function $\alpha(|x' - x|, \tau)$ and calculate the triple integral of Eq. (5). In 1983, Eringen [11] has developed more practical differential forms. The kernel function is determined by matching the lattice dynamics with nonlocal elasticity of Eringen and given by the following form:

$$\alpha(|x' - x|, \tau) = \frac{1}{2\pi d^2 \tau^2} K_0\left(\frac{|x'-x|}{l\tau}, \frac{e_0 a}{l}\right) \tag{6}$$

where K_0 is the modified Bessel function which represents the integral constitutive relation in an equivalent differential form as follows:

$$(1 - (e_0 a)^2 \nabla^2) \sigma_{mn}^{nl} = C_{mnkl} \varepsilon_{kl} \tag{7}$$

The nonlocal Hooke's law for the stress and strain relation is expressed by:

$$\begin{aligned} \sigma_{xx} - (e_0 a)^2 \nabla^2 \sigma_{xx} &= \frac{E}{1-\nu^2} \varepsilon_{xx} + \frac{\nu E}{1-\nu^2} \varepsilon_{\theta\theta} \\ \sigma_{\theta\theta} - (e_0 a)^2 \nabla^2 \sigma_{\theta\theta} &= \frac{\nu E}{1-\nu^2} \varepsilon_{xx} + \frac{E}{1-\nu^2} \varepsilon_{\theta\theta} \\ \sigma_{x\theta} - (e_0 a)^2 \nabla^2 \sigma_{x\theta} &= \frac{E}{1-\nu^2} \frac{(1-\nu)}{2} \gamma_{x\theta} \end{aligned} \tag{8}$$

From equations (2) and (8), the nonlocal constitutive relations of Donnell shell become:

$$\begin{aligned} (1 - (e_0 a)^2 \nabla^2) N_x &= C(\varepsilon_{xx} + \nu \varepsilon_{\theta\theta}) \\ (1 - (e_0 a)^2 \nabla^2) N_\theta &= C(\varepsilon_{\theta\theta} + \nu \varepsilon_{xx}) \\ (1 - (e_0 a)^2 \nabla^2) N_{x\theta} &= \frac{C}{2}(1 - \nu) \gamma_{x\theta}) \end{aligned} \tag{9}$$

and

$$\begin{aligned} (1 - (e_0 a)^2 \nabla^2) M_x &= -D\left(\frac{\partial^2 w}{\partial x^2} + \frac{\nu}{R^2} \frac{\partial^2 w}{\partial \theta^2}\right) \\ (1 - (e_0 a)^2 \nabla^2) M_\theta &= -D\left(\nu \frac{\partial^2 w}{\partial x^2} + \frac{1}{R^2} \frac{\partial^2 w}{\partial \theta^2}\right) \\ (1 - (e_0 a)^2 \nabla^2) M_{x\theta} &= -\frac{D}{R}(1 - \nu) \frac{\partial^2 w}{\partial x \partial \theta}\Bigg) \end{aligned} \tag{10}$$

where C and D are extensional and bending stiffness rigidities of the shell given by:

$$C = \frac{Eh}{1 - \nu^2}, \quad D = \frac{Eh^3}{12(1 - \nu^2)} \tag{11}$$

Multiplying the operator $(1 - (e_0 a)^2 \nabla^2)$ by the third equation of system (3), we obtain:

$$\begin{aligned} &\frac{\partial^2}{\partial x^2}\left[(1 - (e_0 a)^2 \nabla^2) M_x\right] + \frac{2}{R} \frac{\partial^2}{\partial x \partial \theta}\left[(1 - (e_0 a)^2 \nabla^2) M_{x\theta}\right] \\ &\quad + \frac{1}{R^2} \frac{\partial^2}{\partial \theta^2}\left[(1 - (e_0 a)^2 \nabla^2) M_\theta\right] + (1 - (e_0 a)^2 \nabla^2) \\ &\quad \left[\frac{N_\theta}{R} + N_x \frac{\partial^2 w}{\partial x^2} + \frac{2N_{x\theta}}{R} \frac{\partial^2 w}{\partial x \partial \theta} + \frac{N_\theta}{R^2} \frac{\partial^2 w}{\partial \theta^2} + p\right] = 0 \end{aligned} \tag{12}$$

which leads to:

$$\begin{aligned} &k^2 \Delta^2 w - (1 - (e_0 a)^2 \nabla^2) \\ &\quad \left[\rho \frac{N_\theta}{Eh} + \frac{1}{Eh}\left(N_x \frac{\partial^2 w}{\partial x^2} + 2\frac{N_{xy}}{R} \frac{\partial^2 w}{\partial x \partial \theta} + \frac{N_\theta}{R^2} \frac{\partial^2 w}{\partial \theta^2}\right) + \frac{p}{Eh}\right] = 0 \end{aligned} \tag{13}$$

where $k^2 = D/Eh$, $\rho = 1/R$ is the curvature.

To investigate the possible existence of an adjacent equilibrium configurations, we use the adjacent equilibrium criterion [4]. We examine the two adjacent configurations represented by the displacements before and after increments as in the reference [43]. We consider that the

indices 0 and b indicate respectively the pre-buckling and post-buckling quantities. According to the shell theory, the membrane forces N_{xb}, $N_{\theta b}$ and $N_{x\theta b}$ are connected to the stress function Φ $\left(N_x = \frac{Eh}{R^2}\frac{\partial^2\phi}{\partial\theta^2}, N_\theta = Eh\frac{\partial^2\phi}{\partial x^2}, N_{x\theta} = \frac{Eh}{R}\frac{\partial^2\phi}{\partial x\partial\theta}\right)$. Neglecting the terms of second order in index b, we obtain the following equation:

$$k^2\Delta^2 w_b - (1-(e_0a)^2\nabla^2)\left[\rho\frac{\partial^2\Phi}{\partial x^2} + \frac{1}{Eh}\left(N_{x0}\frac{\partial^2 w_b}{\partial x^2} + 2\frac{N_{x\theta 0}}{R}\frac{\partial^2 w_b}{\partial x\partial\theta} + \frac{N_{\theta 0}}{R^2}\frac{\partial^2 w_b}{\partial\theta^2}\right) + \frac{p_b}{Eh}\right] = 0 \tag{14}$$

The stress function $\Phi(x,\theta)$ verifies the following compatibility condition :

$$\Delta^2\phi + \rho\frac{\partial^2 w_b}{\partial x^2} + (e_0a)^2\left[3\rho^2\frac{\partial^6\phi}{\partial x^4\partial\theta^2} + 3\rho^4\frac{\partial^6\phi}{\partial x^6} + \rho^6\frac{\partial^6\phi}{\partial\theta^6}\right] = 0 \tag{15}$$

If the shear membrane forces are neglected $N_{x\theta 0} = 0$, the axial compression is $N_{x0} = P$ and the circumferential membrane force is $N_{\theta 0} = F$, the system (14)–(15) giving the Donnell equations becomes:

$$\begin{aligned} &k^2\Delta^2 w_b - (1-(e_0a)^2\nabla^2)\left[\rho\frac{\partial^2\phi}{\partial x^2} + \left(\lambda\frac{\partial^2 w_b}{\partial x^2} + \frac{F}{R^2}\frac{\partial^2 w_b}{\partial\theta^2}\right) + \frac{p_b}{Eh}\right] = 0 \\ &\Delta^2\phi + \rho\frac{\partial^2 w_b}{\partial x^2} + (e_0a)^2\left[3\rho^2\frac{\partial^6\phi}{\partial x^4\partial\theta^2} + 3\rho^4\frac{\partial^6\phi}{\partial x^6} + \rho^6\frac{\partial^6\phi}{\partial\theta^6}\right] = 0 \end{aligned} \tag{16}$$

where $\lambda = \frac{P}{Eh}$ is the load parameter.

Note that when $e_0 = 0$, the system of coupled equations (14) reduces to the classical (local) Donnell equilibrium equations in which the effect of small length scale is neglected.

2.3 Discussion on the nonlocal parameter e_0 of the nonlocal theory

The characteristic length e_0, of nonlocal continuum mechanics for modeling carbon nanotubes, identifies the nonlocal effect in the analysis. It is determined by experience or by the intersection of dispersion curves for the planes wave with those of lattice dynamics. Eringen [11] defines e_0 as a constant appropriate to each material and finds $e0 = 0.39$, for some materials, by a comparison between the results of lattice dynamics and the nonlocal elasticity theory. Zhang et al. [54] estimated the value of the nonlocal parameter, using the curve fitting of the results of nonlocal elasticity theory to those of molecular mechanics simulations, for the critical buckling strain of SWCNTs under axial compression. Sears and Batra [41] compared their molecular mechanics results to these of nonlocal cylindrical shell model based on the Donnell shell theory to show that $e_0 = 0.82$. Zhang et al. [55] determined that the values of e_0 varied between 0.546 and 1.043 for different chiral angles using the curve fitting of the molecular dynamics simulation results and those of nonlocal cylindrical shell model based on the Donnell shell theory. Wang and Hu [47] obtained the value of e_0 by comparing of the gradient method with atomic lattice dynamics of a one-dimensional lattice. Figure 2 [51] shows the dispersion of a crystal for the one-dimensional lattice where c_0 is the equivalent sound velocity in the crystal, c is the phase velocity in the lattice and k is the lattice wavenumber.

The results of the gradient method are in excellent agreement with the dispersion curves obtained via the Born-Karman model of lattice dynamics particularly at smaller values of ka. There is an other work on the estimated of the parameter e_0 [41, 47, 49, 50, 54, 55]. Different values of the non-local parameter are used in literature. Hussain et al. [16] discussed the nonlocal effect on the vibration of armchair and zigzag SWCNTs with different values of the nonlocal parameter $e_0 = 0.5, 1, 1.5$ and 2. The same values are used by Amara et al. [3] for the buckling studies of MWCNTs under temperature field. Kiani [18–20] showed his results using different small scale parameters e_0a between 0 and $2nm$.

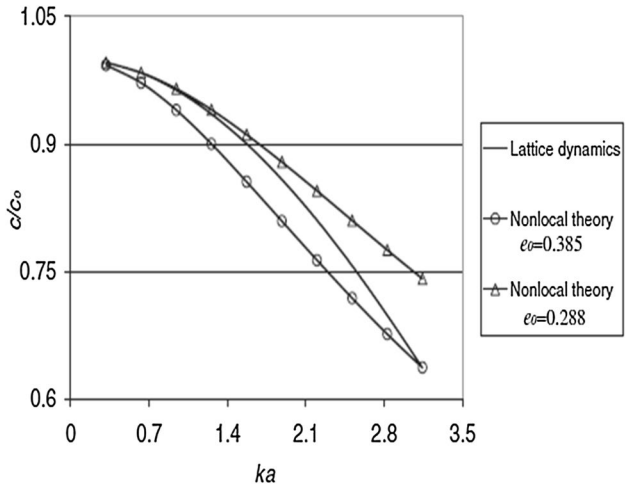

Fig. 2 Dispersion curves of one-dimensional lattice [51]

3 Multiple Donnell shells continuum approach

Consider a multi-walled carbon nanotube (MWCNT), consisting of N tubes of radius $R_j(j = 1;2;...;N)$, length L, same thickness h and Young's modulus E. It subjected to an axial compression P. The walls of adjacent tubes interact through Van der Waals forces as shown in Fig. 3.

Using the continuum Donnell concentric multi-shells, each tube $j(j = 1, 2, ., N)$ is modeled by an elastic homogeneous and isotropic circular cylindrical shell of length L, thickness h, radius R_j, Young's modulus E and Poisson's ratio ν. The considered circular cylindrical shells are coupled by Van der Waals interaction. We denote by $u_i(x,\theta), v_i(x,\theta)$ and $w_i(x,\theta)$, the components of displacement vector with x and θ are the axial and circumferential coordinates respectively. According to Sect. 2.2, the transverse displacement $w_i(x,\theta)$ and the corresponding stress functions $\Phi_j(x,\theta)$ are solutions of the following nonlocal Donnell shell equilibrium equation:

$$\begin{aligned} &k^2\Delta_j^2 w_j - (1-(e_0a)^2\nabla_j^2)\left[\lambda\frac{\partial^2 w_j}{\partial x^2} + \rho_j\frac{\partial^2\phi_j}{\partial x^2} + \frac{F_j^{vdw}}{Eh}\right] = 0 \\ &\Delta_j^2\phi_j + \rho_j\frac{\partial^2 w_j}{\partial x^2} + (e_0a)^2\left[3\rho^2\frac{\partial^6\phi}{\partial x^4\partial\theta^2} + 3\rho^4\frac{\partial^6\phi}{\partial x^6} + \rho^6\frac{\partial^6\phi}{\partial\theta^6}\right] = 0 \end{aligned} \tag{17}$$

where $j = 1, 2, ..., N$, $\rho_j = \frac{1}{R_j}$ is the curvature radius of j^{th} tube, $\Delta_j^2 = \left(\frac{\partial^2}{\partial x^2} + \rho_j^2\frac{\partial^2}{\partial\theta^2}\right)^2$ is the bi-laplacian operator, ϕ_j is the stress function of j^{th} tube. The Van der Waals force F_j^{vdw} is expressed by:

$$F_j^{vdw} = \frac{F_j}{R_j^2}\frac{\partial^2 w_j}{\partial\theta^2} - p_j \tag{18}$$

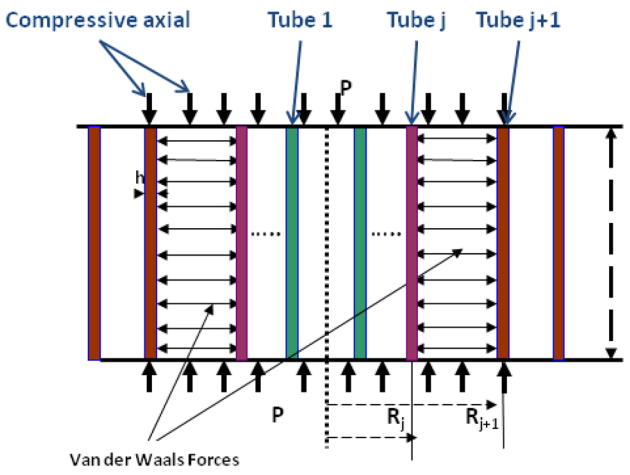

Fig. 3 Multi-walled carbone nanotube (MWCNT) under axial compression

with F_j are the forces by the length unit, prior buckling, in the circumferential direction of tube j and p_j is the Van der Waals interaction between the tubes of MWCNT which is written in the form:

$$p_j = \sum_{k=1}^{N}(w_j - w_k)c_{jk} \tag{19}$$

with c_{jk} are the Van der Waals coefficients given by :

$$c_{jk} = -\left[\frac{1001\pi\epsilon\sigma^{12}}{3a^4}E_{jk}^{13} - \frac{1120\pi\epsilon\sigma^6}{9a^4}E_{jk}^{7}\right]R_k \tag{20}$$

and E_{jk}^m the elliptic integrals expressed as:

$$E_{jk}^m = \frac{1}{(R_j+R_k)^m}\int_0^{\frac{\pi}{2}}\frac{d\theta}{(1-K_{jk}cos^2(\theta))^{m/2}}R_k \tag{21}$$

with a is the length of the C–C bond, ϵ is the depth of Lennard–Jones potential, σ is a parameter being determined by the equilibrium distance and K_{ii} defined by:

$$K_{jk} = \frac{4R_jR_k}{(R_j+R_k)^2} \tag{22}$$

Putting

$\mu = e_0a$ and taking into account of Eqs. (18) and (19) can be written as:

$$\begin{aligned} &k^2\Delta_j^2 w_j - (1-\mu^2\nabla_j^2)\left[\lambda\frac{\partial^2 w_j}{\partial x^2} + \rho_j\frac{\partial^2\phi_j}{\partial x^2}\right. \\ &\left.+\frac{1}{Eh}\left(\frac{F_j}{R_j^2}\frac{\partial^2 w_j}{\partial\theta^2} + \sum_{k=1}^{N}(w_j - w_k)c_{jk}\right)\right] = 0 \\ &\Delta_j^2\phi_j + \rho_j\frac{\partial^2 w_j}{\partial x^2} + (e_0a)^2\left[3\rho^2\frac{\partial^6\phi}{\partial x^4\partial\theta^2}\right. \\ &\left.+3\rho^4\frac{\partial^6\phi}{\partial x^6} + \rho^6\frac{\partial^6\phi}{\partial\theta^6}\right] = 0 \end{aligned} \tag{23}$$

where $j = 1, 2, ..., N$.

4 Buckling analysis of double-walled carbon nanotubes (DWCNTs)

4.1 Buckling load λ

The solution of the problem (23) is sought in the following form:

$$\begin{aligned} w_j(x,\theta) &= A_j exp\left(i\frac{m\pi}{L}x\right)cos(n\theta) + cc \\ &\qquad j = 1, 2, 3, ..., N \\ \phi_j(x,\theta) &= a_j exp\left(i\frac{m\pi}{L}x\right)cos(n\theta) + cc \end{aligned} \tag{24}$$

where m and n are respectively the axial and circumferential half wavenumbers of the j^{th} tube, A_j and a_j are arbitrary complex constants and cc denotes the complex conjugate. As a special case $N = 2$ (DWCNT), the substitution of Eq. (24) in Eq. (23) gives :

$$j=1\begin{cases} k^2\left(p^2+q_1^2\right)^2A_1-\lambda\left[p^2+\mu^2p^2\left(p^2+q_1^2\right)\right]A_1 \\ \quad+\frac{c_{12}}{Eh}\left[\left(1+\mu^2\left(p^2+q_1^2\right)\right)A_2-\left(1+\mu^2\left(p^2+q_1^2\right)\right)A_1\right] \\ \quad-\frac{F_1}{Eh}\left[q_1^2-\mu^2q_1^2\left(p^2+q_1^2\right)\right]A_1 \\ \quad+\rho_1\left[p^2+\mu^2p^2\left(p^2+q_1^2\right)\right]a_1=0 \\ \\ \left(p^2+q_1^2\right)a_1+\mu^2\left[3q_1^2p^4+3q_14p^2+p^6+q_1^6\right]a_1 \\ \quad-p^2A_1=0 \end{cases} \tag{25}$$

and

$$for\quad j=2\begin{cases} k^2\left(p^2+q_2^2\right)^2A_2-\lambda\left[p^2+\mu^2p^2\left(p^2+q_2^2\right)\right]A_2 \\ \quad+\frac{c_{21}}{Eh}\left[\left(1+\mu^2\left(p^2+q_2^2\right)\right)A_2-\left(1+\mu^2\left(p^2+q_2^2\right)\right)A_1\right] \\ \quad-\frac{F_2}{Eh}\left[q_2^2-\mu^2q_2^2\left(p^2+q_2^2\right)\right]A_2 \\ \quad+\rho_2\left[p^2+\mu^2p^2\left(p^2+q_2^2\right)\right]a_2=0 \\ \left(p^2+q_2^2\right)a_2+\mu^2\left[3q_2^2p^4+3q_2^4p^2+p^6+q_2^6\right]a_2 \\ \quad-p^2A_2=0 \end{cases} \tag{26}$$

where $p = m\pi/L$ and $q_j = n/R_j$.

The second equations in systems (25) and (26) lead to:

$$\begin{aligned} a_1&=\frac{p^2A_1}{\left(p^2+q_1^2\right)^2+\mu^2\left(3q_1^2p^4+3q_1^4p^2+p^6+q_1^6\right)} \\ a_2&=\frac{p^2A_2}{\left(p^2+q_2^2\right)^2+\mu^2\left(3q_2^2p^4+3q_2^4p^2+p^6+q_2^6\right)} \end{aligned} \tag{27}$$

Inserting (27) in the first equations of the system (25) and (26), we obtain the following system:

$$\begin{aligned} &\left[\alpha_1-\lambda p^2\left(1+\mu^2p^2\left(1+\beta_1^2\right)\right)\right]A_1 \\ &\quad+\frac{c_{12}}{Eh}\left[1+\mu^2p^2\left(1+\beta_1^2\right)\right]A_2=0 \\ &\frac{c_{12}}{Eh}\left[1+\mu^2p^2\left(1+\beta_2^2\right)\right]A_1 \\ &\quad+\left[\alpha_2-\lambda p^2\left(1+\mu^2p^2\left(1+\beta_2^2\right)\right)\right]A_2=0 \end{aligned} \tag{28}$$

where $\beta_1 = q_1/p$ and $\beta_2 = q_2/p$ are the aspect ratios, α_1 and α_2 are expressed by:

$$\begin{aligned} \alpha_1&=k^2\left(1+\beta_1^2\right)^2p^4+\frac{\rho_1\left(1+\mu^2p^2\left(1+\beta_1^2\right)\right)}{\left(1+\beta_1^2\right)^2+\mu^2p^2\left(3\beta_1^2+3\beta_1^4+\beta_1^6+1\right)} \\ &\quad-\frac{c_{12}}{Eh}\left(1+\mu^2p^2\left(1+\beta_1^2\right)\right)-\frac{F_1}{Eh}\beta_1^2\left(1-\mu^2p^4\left(1+\beta_1^2\right)\right) \\ \alpha_2&=k^2\left(1+\beta_2^2\right)^2p^4+\frac{\rho_2\left(1+\mu^2p^2\left(1+\beta_2^2\right)\right)}{\left(1+\beta_2^2\right)^2+\mu^2p^2\left(3\beta_2^2+3\beta_2^4+\beta_2^6+1\right)} \\ &\quad-\frac{c_{21}}{Eh}\left(1+\mu^2p^2\left(1+\beta_2^2\right)\right)-\frac{F_2}{Eh}\beta_2^2\left(1-\mu^2p^4\left(1+\beta_2^2\right)\right) \end{aligned} \tag{29}$$

The system (28) has non-trivial solution A_1 and A_2 if its determinant is zero. This requirement is the buckling condition which leads to:

$$\left(X_0p^4\right)\lambda^2-X\lambda+Y=0 \tag{30}$$

where

$$\begin{aligned} X_0&=\left(1+\mu^2p^2\left(1+\beta_1^2\right)\right)\left(1+\mu^2p^2\left(1+\beta_2^2\right)\right) \\ X&=p^2\left[\alpha_1\left(1+\mu^2p^2\left(1+\beta_2^2\right)\right)\right. \\ &\quad\left.+\alpha_2\left(1+\mu^2p^2\left(1+\beta_1^2\right)\right)\right] \\ Y&=\alpha_1\alpha_2-\frac{c_{12}c_{21}}{(Eh)^2}\left(1+\mu^2p^2\left(1+\beta_1^2\right)\right) \\ &\quad\times\left(1+\mu^2p^2\left(1+\beta_2^2\right)\right) \end{aligned} \tag{31}$$

The solution of (30) gives the expression of the buckling load:

$$\lambda=\frac{X-\sqrt{X^2-4X_0Yp^4}}{2X_0p^4} \tag{32}$$

This root is obtained by taking the negative sign before the square-root. The expression (32) can be written according to m and n ($\lambda(m,n)$) and it can also be written according to β_1, β_2 and p ($\lambda(\beta_1,\beta_2,p)$) in the following compact form:

$$\begin{aligned} &\lambda(\beta_1,\beta_2,p) \\ &\quad=\frac{1}{2p^2\zeta_1\zeta_2}\left(\alpha_1\zeta_2+\alpha_2\zeta_1-\sqrt{\left(\alpha_1\zeta_2+\alpha_2\zeta_1\right)^2+Z}\right) \end{aligned} \tag{33}$$

where

$$\begin{aligned} \zeta_1&=\left(1+\mu^2p^2\left(1+\beta_1^2\right)\right) \\ \zeta_2&=\left(1+\mu^2p^2\left(1+\beta_2^2\right)\right) \\ Z&=4\zeta_1\zeta_2\left(\zeta_1\zeta_2\frac{c_{12}c_{21}}{(Eh)^2}-\alpha_1\alpha_2\right) \end{aligned} \tag{34}$$

The minimization of the buckling load ($\lambda(m,n)$), by searching numerically the values of m and n, allows to obtain the critical buckling load of the double-walled carbon nanotubes as in [17, 37]. This method is very expensive and does not give a good precision. In the next section, we propose a novel approach for determination of the nonlocal critical buckling load of DWCNTs for a fixed aspect ratio β_1 and β_2 and with respect to the wave of axial number p. To validate the proposed approach, we compare the results

with those obtained by the minimization procedure of the buckling load ($\lambda(m,n)$) with respect to the integer numbers m and n.

4.2 Proposed approach for the nonlocal critical buckling load of the DWCNTs

The numerical experiments show that the relative error of the critical buckling load $\lambda_{cr}(p_{cr})$, using the equation (33), decreases as the axial wave number p increases at the beginning. Continuously increasing p, the relative error of λ_{cr} becomes larger and gives an incorrect result for larger p. By considering these remarks as shown in reference [17] and in order to find p_{cr} quickly, we propose the following algorithm:

$$
\begin{aligned}
&d = 2\\
&S = 100\\
&\epsilon = 0.05\\
&\lambda_{cr}^{0} = 0.0001\\
&p = p_{prediction}\\
&error1 = 4\\
&error2 = 3\\
&error3 = 2\\
&error4 = 1\\
&\\
&for\ i = 0 : d\\
&\quad for j = 1 : S\\
&\quad\quad p_j^i = p + j10^{-i}\\
&\quad end\\
&\\
&\quad n = 0\\
&\quad while(min(error3, error4) < min(error1, error2))\\
&\quad\quad n = n + 1\\
&\quad\quad \lambda_{cr}^{n} = \lambda(p_n^i) \quad (see\ Eq.(33))\\
&\quad\quad error(p_n^i) = |\frac{\lambda_{cr}^{(n-1)} - \lambda_{cr}^{n}}{\lambda_{cr}^{(n-1)}}|\\
&\quad\quad error1 = error2\\
&\quad\quad error2 = error3\\
&\quad\quad error3 = error4\\
&\quad\quad error4 = error(m_n^i)\\
&\quad end\\
&\\
&\quad if\,(n - 3 > 0)\\
&\quad\quad p = p_{n-3}^i + \epsilon\\
&\quad else\\
&\quad\quad p = p_1^i - 10^{-i}\\
&\quad end\\
&\\
&end\\
&p_{cr} = p\\
&\lambda_{cr} = \lambda(p_{cr}) \quad (see\ Eq.(33))
\end{aligned}
\tag{35}
$$

where d denotes the accuracy of p_{cr} to the mth decimal place, ϵ is related to the starting point of the test scope and gets a value between 0 and 1.

5 Numerical analysis for the critical buckling load of DWCNTs

Numerical results are presented in this section for validating the proposed approach of the nonlocal critical buckling load of DWCNTs under axial compression. In these numerical tests, data of double Donnell shells model are given as follows: the inner diameter $R_1 = 2$ nm, the median inter-shell spacing between carbon of DWCNTs $\delta R = 0.34$, the aspect ratios (length to radius) $L/R_1 = 10$, $h = 0.066$ nm, $a = 0.142$ nm, $E = 5500\,GPa$, $\upsilon = 0.34$, $c_{12} = \frac{-320\times10^{-3}}{0.16a^2}$nN/nm^3, $c_{21} = (R_1/R_2)c_{12}$, $F_1 = 0$, $e_0 = 0.39$ [11, 15, 52]. The validation process consists in comparing the results of minimizing the buckling load ($\lambda(m,n)$) and those of the proposed approach (35) with fixed values of aspect ratios β_1 and β_2.

The buckling load $\lambda(m,n)$, for the nonlocal parameter $e_0 = 0.39$, are plotted in Fig. 4 versus the half-wave numbers in the axial and circumferential directions (m,n).

To validate the proposed approach of the nonlocal critical buckling load, we consider the values of aspect ratios $\beta_1 = 0.72$ and $\beta_2 = 0.62$ which are equivalent to the critical values $(m = 22, n = 5)$ as a shown in Fig. 4. The chosen parameters of the proposed approach are $d = 2$, $S = 100$, $\epsilon = 0.01$, $p_{prediction} = 0$ and $\lambda_{cr}^{0} = 0.0001$. Using the proposed approach (see Eq. (35)), Fig. 5 represent the first estimate ($i = 0$) of the critical wave number p_{cr} in axial direction, by plotting the variation of the relative error variation versus the wave number p in axial direction, which gives a value between 3nm^{-1} and 4nm^{-1}.

So, in the second estimate ($i = 1$), we are looking for precision in the interval [3nm^{-1}, 4nm^{-1}] or the accuracy of p_{cr} to the first decimal place as shown the Fig. 6.

In the same way in the interval [3.3nm^{-1}, 3.4nm^{-1}] as you can see in the Fig. 7, the accuracy of p_{cr} to the second decimal place gives the critical wave number $p_{cr} = 3.38nm^{-1}$ which is equivalent to the critical buckling load $\lambda_{cr} = 0.01775$ with the relative error $10^{-3}\%$. This critical value is equal to the minimum value of the critical buckling load of the curve given by minimizing numerically $\lambda(m,n)$. We can note that the proposed approach allows to determine the critical load according to aspect

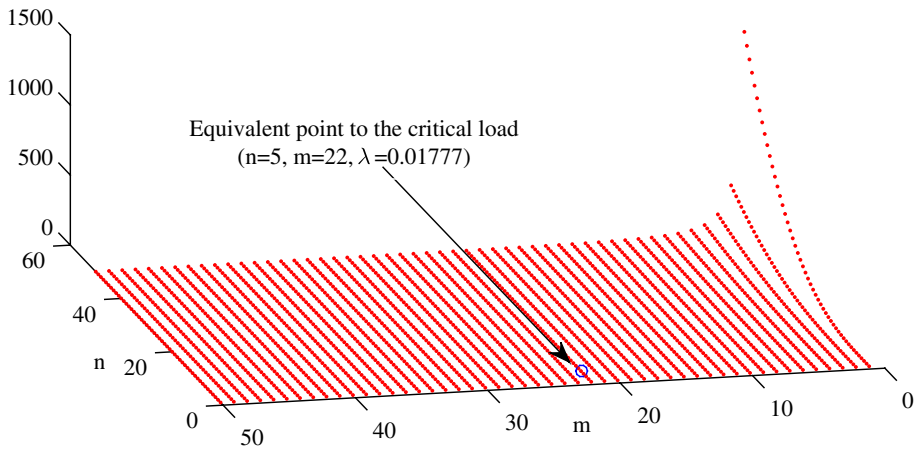

Fig. 4 Buckling loads λ versus (m, n) for the nonlocal parameter $e_0 = 0.39$

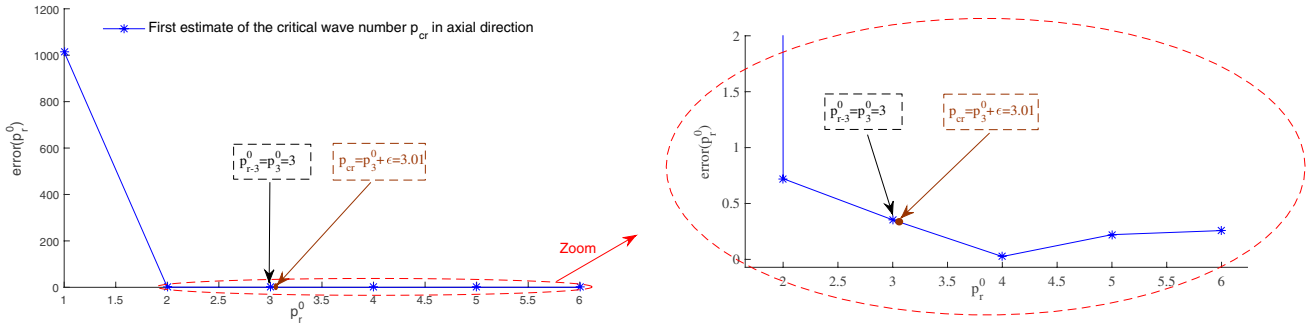

Fig. 5 Relative error variation versus the wave number p in axial direction for the first estimate where $(i = 0)$ and $r = 6$

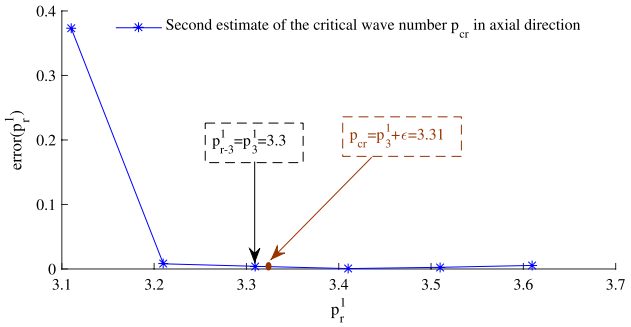

Fig. 6 Relative error variation versus the wave number p in axial direction for the second estimate where $(i = 1)$ and $r = 6$

ratios with good precision and according to the quality requested by the user. In the following we will present some tests using the proposed approach (see Eq. (35)) to show the influence of various parameters on the critical load λ_{cr}.

The critical buckling load of DWCNTs decreases when the nonlocal parameter e_0 increase as shown in the Fig. 8 which shows that we cannot neglect the effect of small scales especially for the great values of e_0. Secondly, these results demonstrate that the approximation given by Ru [37], in which the ratio $(R_2 - R_1)/R_1$ is neglected, provides a higher critical buckling load.

In Fig. 9, we plot the critical buckling load versus the aspect ratio for a fixed force $F_1 = 0$ and different nonlocal parameters e_0. It is clear that for $F_1 = 0$ and a fixed nonlocal parameter, λ_{cr} increases with increasing values of aspect ratio β_1. We can also notice that for $F_1 = 0$ and a fixed aspect ratio β_1, λ_{cr} decreases with increasing values of nonlocal parameter e_0.

Now we are interested to study the effect of the force F_1 for a fixed nonlocal parameter as shown in Figs. 10 and 11. These graphs show that, for each value of the nonlocal parameter, there is a certain value F of the force F_1 such that for all force F_1 greater than F, the critical buckling load parameter in terms of the aspect ratio presents a maximum and decreases from this aspect ratio corresponding to this maximum. Below this value leads to the increasing of λ_{cr} with increasing the aspect ratio. Analysis of the results shows that the value of F increases with increasing values of the nonlocal parameter e_0.

In Fig. 12, we draw the critical buckling load of DWCNTs versus the aspect ratio $(R_2 - R_1)/R_1$ for some nonlocal

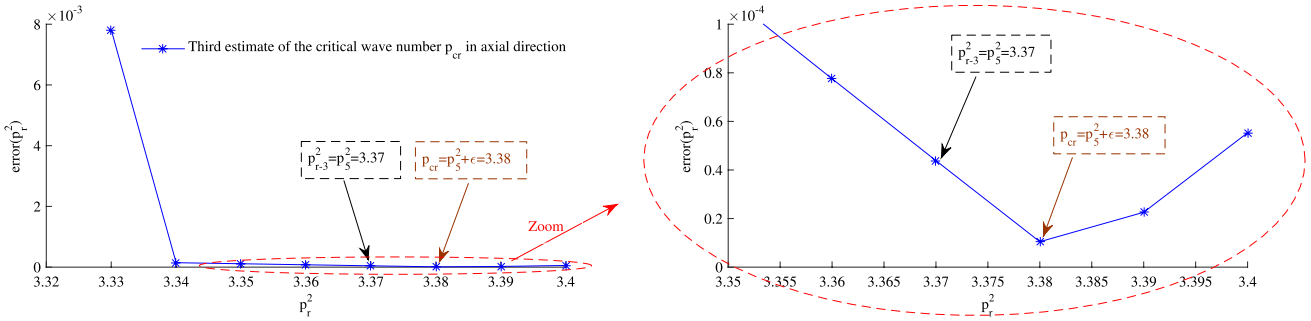

Fig. 7 Relative error variation versus the wave number p in axial direction for the third estimate where ($i = 2$) and $r = 8$

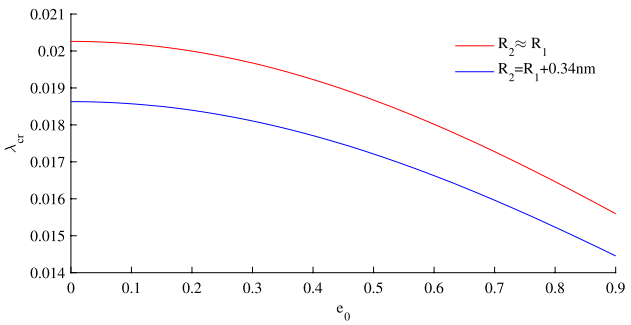

Fig. 8 Critical buckling load versus the nonlocal parameter e_0 for equal and different radii

parameters values $e_0 = 0.39$, $e_0 = 0.5$ and $e_0 = 0.7$ where the force $F_1 = 0$. This figure indicates that the critical buckling load increases with increasing values of the ratio $(R_2 - R_1)/R_1$. The same observation remains true whatever the value of the force F_1 as shown in the Fig. 13.

6 Conclusion

An approach of the nonlocal critical buckling load of double-walled carbon naotube (DWCNTs) under axial compression for fixed values of aspect ratios has been developed. The derivation of the proposed approach is performed using the nonlocal multiple Donnell shells continuum approach without any assumption over tubes radii. This proposed solution approach permits to take into consideration the small scale effects using the nonlocal elasticity theory of Eringen and the median intershell spacing which their omission leads to an overestimation of the critical buckling load. We can observe in the numerical applications that the small scale effect becomes very important with increasing the nonlocal parameter e_0 which leads to a lower critical buckling load. On the other hand, this critical buckling load increases with increasing of the aspect ratio $\beta = \frac{L/m\pi}{R/n}$

Fig. 9 Critical buckling load versus the aspect ratio β_1 for a fixed force $F_1 = 0$ and different nonlocal parameters e_0

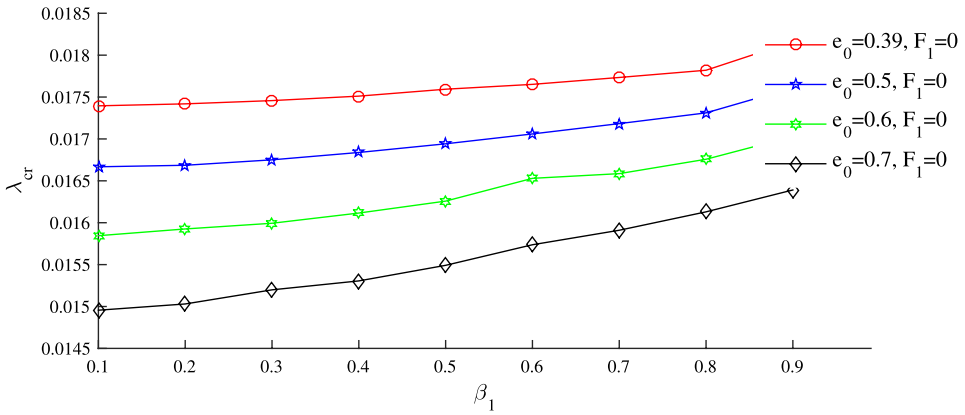

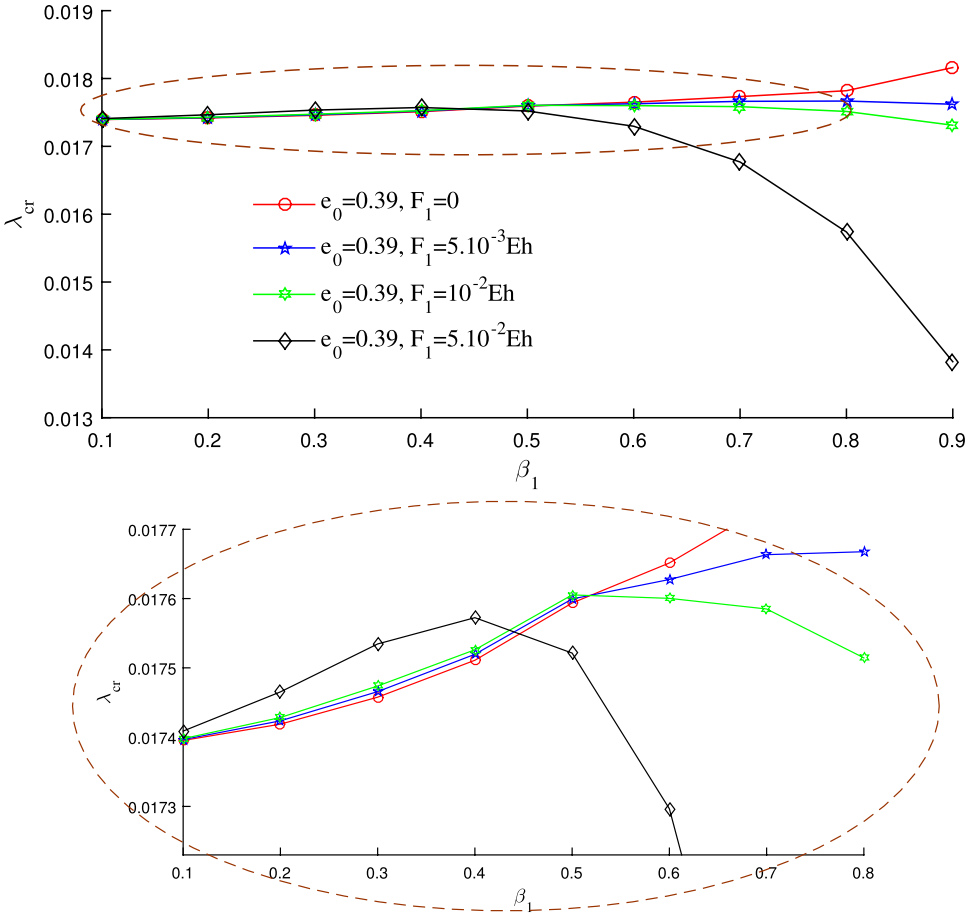

Fig. 10 Critical buckling load versus the aspect ratio β_1 for a fixed nonlocal parameter $e_0 = 0.39$ and different values of the force F_1

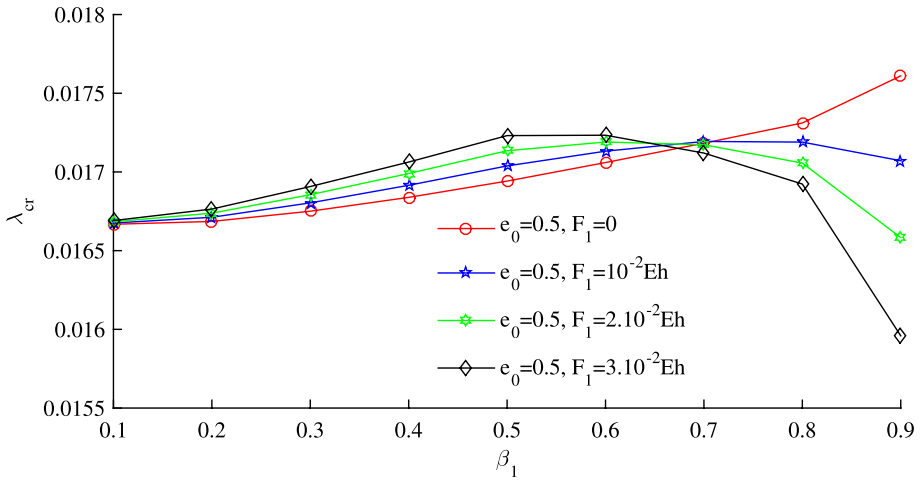

Fig. 11 Critical buckling load versus the aspect ratio β_1 for a fixed nonlocal parameter $e_0 = 0.5$ and different values of the force F_1

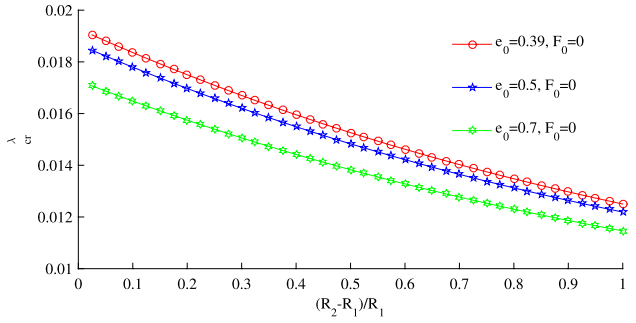

Fig. 12 Critical buckling load versus the ratio $(R_2 - R_1)/R_1$ for a fixed force $F_1 = 0$ and different nonlocal parameters $e_0 = 0.39$, $e_0 = 0.5$ and $e_0 = 0.7$

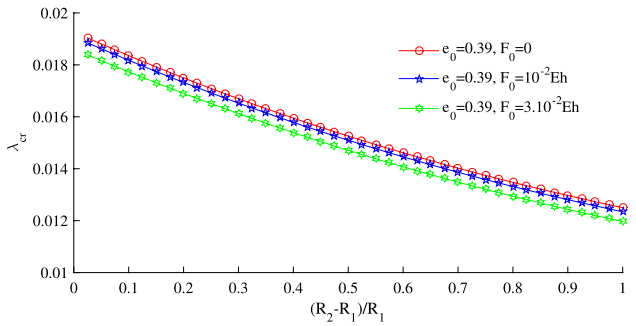

Fig. 13 Critical buckling load versus the ratio $(R_2 - R_1)/R_1$ for a fixed nonlocal parameter e_0 and different forces $F_1 = 0$, $F_1 = 10^{-2}Eh$ and $F_1 = 3.10^{-2}Eh$

(long axial wavelengths/circumferential wavelengths). But there is a certain value F of the force F_1 from which the critical buckling load accept a maximum in terms of the aspect ratio β, from the correspond aspect ratio to this maximum the critical buckling load decreases.

Compliance with ethical standards

Conflict of interest The authors declare that they have no conflict of interest.

Human and animal rights This article does not contain any studies with human participants or animals performed by the author.

Informed consent No individual participants were included in the study so there are no subjects for which informed consent requirements arise.

References

1. Askes H, Aifantis EC (2009) Gradient elasticity and flexural wave dispersion in carbon nanotubes. Phys Rev B 80:195412
2. Adda Bedia W, Houari MSA, Bessaim A, Bousahla AA, Tounsi A, Saeed T, Alhodaly MS (2019) A new hyperbolic two-unknown beam model for bending and buckling analysis of a nonlocal strain gradient nanobeams. J Nano Res 57:175–191
3. Amara K, Tounsi A, Mechab I, Adda-Bedia E (2010) Nonlocal elasticity effect on column buckling of multiwalled carbon nanotubes under temperature field. Appl Math Model 34:3933–3942
4. Brush D, Almroth B (1975) Buckling of bars, plates and shells. McGraw-Hill, New York
5. Berghouti H, Adda Bedia EA, Benkhedda A, Tounsi A (1975) Vibration analysis of nonlocal porous nanobeams made of functionally graded material. Adv Nano Res 7:351–364
6. Boutaleb S, Benrahou KH, Bakora A, Algarni A, Bousahla AA, Tounsi Aw, Tounsi Ad, Mahmoud SR (2019) Dynamic analysis of nanosize FG rectangular plates based on simple nonlocal quasi 3D HSDT. Adv Nano Res 7:189–206
7. Chen W, Hong Y, Lin J (2018) The sample solution approach for determination of the optimal shape parameter in the multiquadric function of the Kansa method. Comput Math Appl 75:2942–2954
8. Donnell LH (1934) Stability of thin-walled tubes under torsion. N.A.C.A, Technical Report No. 479
9. Draoui A, Zidour M, Tounsi A, Adim B (2019) Static and dynamic behavior of nanotubes-reinforced sandwich plates using (FSDT). J Nano Res 57:117–135
10. Eringen AC (1972) Nonlocal polar elastic continua. Int J Eng Sci 10:1–16
11. Eringen AC (1983) On differential-equations of nonlocal elasticity and solutions of screw dislocation and surface-waves. J Appl Phys 54:4703–4710
12. Eringen AC, Edelen DGB (1972) On nonlocal elasticity. Int J Eng Sci 10:233–248
13. Endo M, Muramatsu H, Hayashi T, Kim YA, Terrones M, Dresselhaus MS (2005) Nanotechnology: 'buckypaper' from coaxial nanotubes. Nature 433:476
14. Falvo MR, Clary GJ, Taylor RM, Chi V, Brooks FP, Washburn S, Superfine R (1997) Bending and buckling of carbon nanotubes under large strain. Nature 389:582–584
15. Gopalakrishan S, Narendar S (2013) Wave propagation in nanostructures. Nonlocal Continuum Mechanics Formulations. Springer, New York
16. Hussain M, Naeem MN, Tounsi A, Taj M (2019) Nonlocal effect on the vibration of armchair and zigzag SWCNTs with bending rigidity. Adv Nano Res 7:431–442
17. He XQ, Kitipornchai S, Liew KM (2005) Buckling analysis of multi-walled carbon nanotubes: a continuum model accounting for van der waals interaction. J Mech Phys Solids 53:303–326
18. Kiani K (2014) Axial buckling analysis of vertically aligned ensembles of single-walled carbon nanotubes using nonlocal discrete and continuous models. Acta Mech 225:3569–3589
19. Kiani K (2015) Nonlocal and shear effects on column buckling of single-layered membranes from stocky single-walled carbon nanotubes. Compos B Eng 79:535–552
20. Kiani K (2015) Axial buckling scrutiny of doubly orthogonal slender nanotubes via nonlocal continuum theory. J Mech Sci Technol 29:4267–4272
21. Kiani K (2016) Elastic buckling of current-carrying double-nanowire systems immersed in a magnetic field. Acta Mech 227:3549–3570

22. Kiani K (2017) Exact postbuckling analysis of highly stretchable-surface energetic-elastic nanowires with various ends conditions. Int J Mech Sci 124:242–252
23. Kiani K (2017) Postbuckling scrutiny of highly deformable nanobeams: a novel exact nonlocal-surface energy-based model. J Phys Chem Solids 110:327–343
24. Karami B, Janghorban M, Tounsi A (2018) Nonlocal strain gradient 3D elasticity theory for anisotropic spherical nanoparticles. Int J Steel Compos Struct 27:201–216
25. Karami B, Janghorban M, Tounsi A (2019) On exact wave propagation analysis of triclinic material using three dimensional bi-Helmholtz gradient plate model. Struct Eng Mech 69:487–497
26. Karami B, Janghorban M, Tounsi A (2019) Wave propagation of functionally graded anisotropic nanoplates resting on Winkler–Pasternak foundation. Struct Eng Mech 7:55–66
27. Karami B, Shahsavari D, Janghorban M, Tounsi A (2019) Resonance behavior of functionally graded polymer composite nanoplates reinforced with graphene nanoplatelets. Int J Mech Sci 156:94–105
28. Li L, Hu Y (2015) Buckling analysis of size-dependent nonlinear beams based on a nonlocal strain gradient theory. Int J Eng Sci 97:84–94
29. Lim C, Zhang G, Reddy J (2015) A higher-order nonlocal elasticity and strain gradient theory and its applications in wave propagation. J Mech Phys Solids 78:298–313
30. Mindlin RD (1964) Microstructure in linear elasticity. Arch Ration Mech Anal 16:51–78
31. Mindlin RD (1965) Second gradient of strain and surface-tension in linear elasticity. Int J Solids Struct 1:417–438
32. Mindlin RD, Eshel NN (1968) On first strain-gradient theories in linear elasticity. Int J Solids Struct 4:109–124
33. Mindlin RD, Tiersten HF (1962) Effects of couple stresses in linear elasticity. Arch Ration Mech Anal 11:415–448
34. Papargyri-Beskou S, Polyzos D, Beskos D (2009) Wave dispersion in gradient elastic solids and structures: a unified treatment. Int J Solids Struct 46:3751–3759
35. Poncharal P, Wang ZL, Ugarte D, De Heer WA (1999) Electrostatic deflexions and electromechanical resonances of carbon nanotubes. Science 283:1513–1516
36. Ru CQ (2000a) Effective bending stiffness of carbon nanotubes. Phys Rev B 62:9973–9976
37. Ru CQ (2000b) Effect of van der Waals forces on axial buckling of a double-walled carbon nanotubes. J Appl Phys 87:7227–7231
38. Ru CQ (2001a) Axially compressed buckling of a double-walled carbon nanotube embedded in an elastic medium. J Mech Phys Solids 49:1265–1279
39. Ru CQ (2001b) Degraded axial buckling strain of multi-walled carbon nanotubes due to interlayer slips. J Appl Phys 89:3426–3433
40. Sudak LJ (2003) Column buckling of multiwalled carbon nanotubes using nonlocal continuum mechanics. J Appl Phys 94:7281–7287
41. Sears A, Batra RC (2004) Macroscopic properties of carbon nanotubes from molecular-mechanics simulations. Phys Rev B 69:235406
42. Semmah A, Heireche H, Bousahla AA, Tounsi A (2019) Thermal buckling analysis of SWBNNT on Winkler foundation by non local FSDT. Adv Nano Res 7:89–98
43. Timesli A, Braikat B, Jamal M, Damil N (2017) Prediction of the critical buckling load of multi-walled carbon nanotubes under axial compression. Comptes Rendus Mécanique 345:158–168
44. Treacy MMJ, Ebbesen TW, Gibson JM (1996) Exceptionally high Young's modulus observed for individual carbon nanotubes. Nature 381:678–680
45. Tlidji Y, Zidour M, Draiche K, Safa A, Bourada M, Tounsi A, Bousahla AA, Mahmoud SR (2019) Vibration analysis of different material distributions of functionally graded microbeam. Struct Eng Mech 69:637–649
46. Wang Q (2005) Wave propagation in carbon nanotubes via nonlocal continuum mechanics. J Appl Phys 98:124301
47. Wang L, Hu H (2005) Flexural wave propagation in single-walled carbon nanotubes. Phys Rev B 71:195412
48. Wong EW, Sheehan PE, Lieber CM (1997) Nanobeam mechanics elasticity, strength, and toughness of nanorods and nanotubes. Science 277:1971–1975
49. Wang Q, Varadan VK, Quek ST (2006) Small scale effect on elastic buckling of carbon nanotubes with nonlocal continuum models. Phys Lett A 357:130–135
50. Wang Q, Varadan VK (2005) Stability analysis of carbon nanotubes via continuum models. Smart Mater Struct 14:281
51. Wang Q, Wang CM (2007) The constitutive relation and small scale parameter of nonlocal continuum mechanics for modelling carbon nanotubes. Nanotechnology 18:075702
52. Wang CM, Zhang YY, Xiang Y, Reddy JN (2010) Recent studies on buckling of carbon nanotubes. Appl Mech Rev 63:030804
53. Yacobson BI, Brabec CJ, Bernhole J (1996) Nanomechanics of carbon nanotubes: instabilities beyound linear response. Phys Rev Lett 76:2511–2514
54. Zhang YQ, Liu GR, Xie XY (2005) Free transverse vibrations of double-walled carbon nanotubes using a theory of nonlocal elasticity. Phys Rev B 71:195404
55. Zhang YY, Tana VBC, Wang CM (2006) Effect of chirality on buckling behavior of single-walled carbon nanotubes. J Appl Phys 100:074304